ARTICLES
PUBLISHED ONLINE: 25 MAY 2015 | DOI: 10.1038/NMAT4295
nature materials

Symmetry of charge order in cuprates

R. Comin[1,2]*, R. Sutarto[3], F. He[3], E. H. da Silva Neto[1,2,4,5], L. Chauviere[1,2,4], A. Fraño[4,6], R. Liang[1,2], W. N. Hardy[1,2], D. A. Bonn[1,2], Y. Yoshida[7], H. Eisaki[7], A. J. Achkar[8], D. G. Hawthorn[8], B. Keimer[4], G. A. Sawatzky[1,2] and A. Damascelli[1,2]*

Charge-ordered ground states permeate the phenomenology of *3d*-based transition metal oxides, and more generally represent a distinctive hallmark of strongly correlated states of matter. The recent discovery of charge order in various cuprate families has fuelled new interest into the role played by this incipient broken symmetry within the complex phase diagram of high-T_c superconductors. Here, we use resonant X-ray scattering to resolve the main characteristics of the charge-modulated state in two cuprate families: $Bi_2Sr_{2-x}La_xCuO_{6+\delta}$ (Bi2201) and $YBa_2Cu_3O_{6+y}$ (YBCO). We detect no signatures of spatial modulations along the nodal direction in Bi2201, thus clarifying the inter-unit-cell momentum structure of charge order. We also resolve the intra-unit-cell symmetry of the charge-ordered state, which is revealed to be best represented by a bond order with modulated charges on the O-2*p* orbitals and a prominent *d*-wave character. These results provide insights into the origin and microscopic description of charge order in cuprates, and its interplay with superconductivity.

Complex oxides exhibit a mosaic of exotic electronic phases with various symmetry-broken ground states that revolve around three main instabilities: antiferromagnetism, charge order and superconductivity. In particular, charge order—the tendency of the valence electrons to segregate into periodically modulated structures—is found in various classes of strongly correlated *3d*-oxides, such as manganites[1], nickelates[2] and cobaltates[3]. The original discovery of period-4 stripe-like charge correlations in the La-based materials[4–7] confirmed the central role played by charge-ordered states in the physics of underdoped cuprates, as anticipated by earlier theoretical work[8–12]. Following further indications by surface-sensitive scanning tunnelling microscopy (STM; refs 13,14), the field was recently revived by the detection of charge-modulated states in YBCO using nuclear magnetic resonance[15] and resonant X-ray scattering (RXS), with wavevector $Q^* \sim 0.31$ reciprocal lattice units (r.l.u., used hereafter)[16–21]. Even more recently, this phenomenology was confirmed in Bi-based materials (with $Q^* \sim 0.26$ and 0.3 in single- and double-layer compounds, respectively), following observations in both bulk/momentum space (with RXS) and surface/real space (with STM; refs 22,23), as well as in the electron-doped $Nd_{2-x}Ce_xCuO_4$, where $Q^* \sim 0.24$ was observed by RXS (ref. 24). These multiple experimental observations establish a ubiquitous instability towards charge ordering in the underdoped cuprates.

The microscopic mechanisms that lead to charge order, and govern its interplay with superconductivity and magnetism, are key to the ultimate understanding of the multiple electronic phases that emerge out of the interaction between charge, spin and lattice degrees of freedom. The relevance of this electronic instability has been extensively pointed out[25,26] and recently resurged as a prominent topic[27–37], sparking an intense debate and urging the need for further experimental investigations of the microscopic structure of the charge-ordered state. Several important questions—such as where charges reside and what is their local symmetry—were recently addressed at both the theoretical[27,28] and experimental level[38,39].

Here we explore the detailed momentum structure of the charge-density-wave (CDW) order $\Delta_{CDW}(\mathbf{k}, \mathbf{Q})$ using RXS, which probes the electronic density directly in reciprocal space, with extreme sensitivity. Our study addresses two major open questions: whether CDW signatures in (Q_x, Q_y) space are found exclusively along the reciprocal-space directions $(Q^*, 0)$ and $(0, Q^*)$, or whether they are also present along (Q^*, Q^*), as discussed in refs 27,28,31,32,34–36; and how charges are distributed spatially, and what is the resulting local symmetry of the ordered state[27–30,36,37]. In more general terms, the first and second questions relate to the **Q**- (inter-unit-cell) and **k**- (intra-unit-cell) dependence of the charge order, respectively.

The first part of this work, aimed at addressing the **Q**-structure of Δ_{CDW}, was performed on the underdoped single-layer compound $Bi_2Sr_{1.2}La_{0.8}CuO_{6+\delta}$ (Bi2201-UD15K), with hole doping $p \sim 0.11$ and $T_c = 15$ K. This material exhibits signatures of incommensurate CDW with wavevectors $(Q^*, 0)$ and $(0, Q^*)$ ($Q^* = 0.265$) (ref. 22). The smaller value of Q^* allows reaching—at the Cu-L_3 edge—momenta located near (Q^*, Q^*) which in contrast are not accessible in double-layer YBCO and $Bi_2Sr_2CaCu_2O_{8+\delta}$. We use RXS (see Methods) to selectively probe the CuO_2-derived electronic states by tuning the photon energy to the Cu-L_3 absorption resonance (Fig. 1a). The corresponding experimental results for the momentum-resolved electronic density in the CuO_2 planes are shown in Fig. 1b for the two high-symmetry directions $(H, 0)$ and (H, H) in the (Q_x, Q_y) plane. Owing to the presence of charge-order peaks, both along $(H, 0)$ and $(0, H)$, the experimental data are compatible with both chequerboard order (bidirectional) or alternating stripes (unidirectional). In the case of bidirectional order, the two simplest modulation patterns of the charge density $\Delta\rho(x, y)$ with wavevector

[1]Department of Physics and Astronomy, University of British Columbia, Vancouver, British Columbia V6T 1Z1, Canada. [2]Quantum Matter Institute, University of British Columbia, Vancouver, British Columbia V6T 1Z4, Canada. [3]Canadian Light Source, Saskatoon, Saskatchewan S7N 2V3, Canada. [4]Max Planck Institute for Solid State Research, Heisenbergstrasse 1, D-70569 Stuttgart, Germany. [5]Quantum Materials Program, Canadian Institute for Advanced Research, Toronto, Ontario M5G 1Z8, Canada. [6]Helmholtz-Zentrum Berlin für Materialien und Energie, Albert-Einstein Straße 15, 12489 Berlin, Germany. [7]National Institute of Advanced Industrial Science and Technology (AIST), Tsukuba 305-8568, Japan. [8]Department of Physics and Astronomy, University of Waterloo, Waterloo N2L 3G1, Canada. *e-mail: r.comin@utoronto.ca; damascelli@physics.ubc.ca

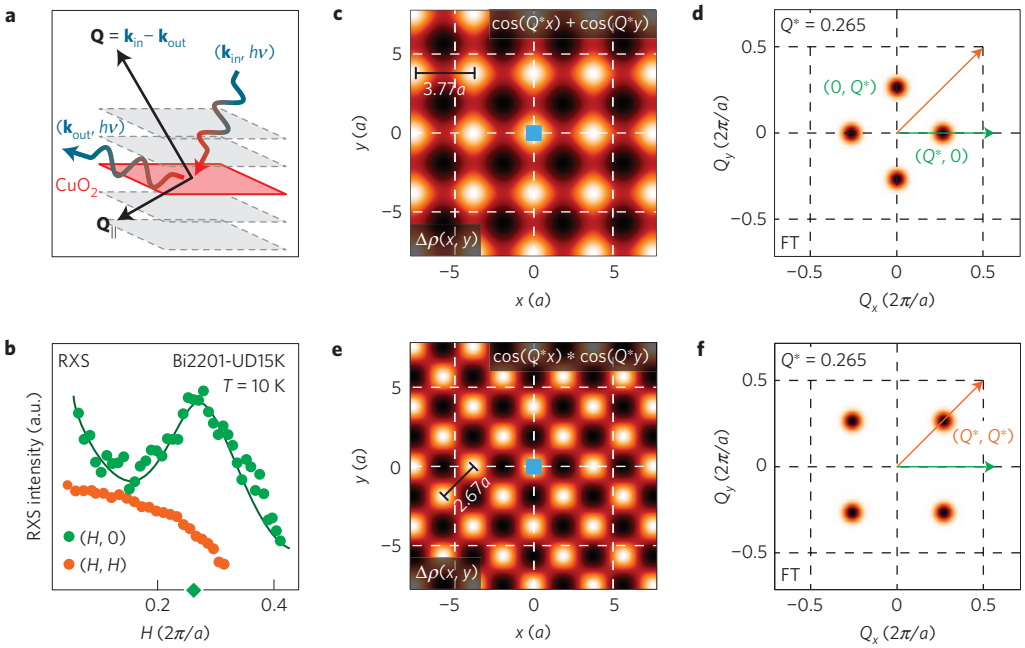

Figure 1 | Charge-ordering patterns and wavevectors. a, Schematics of the RXS experiment. **b**, Low-temperature RXS (at photon energy $h\nu = 931.5$ eV) from an underdoped Bi2201-UD15K sample, mapping reciprocal-space features along the two high-symmetry directions: $(H, 0)$, antinodal, green (reproduced from ref. 22, the full line represents a Gaussian fit plus background); and (H, H), nodal, orange. **c**,**e**, Modulation of the charge density $\Delta\rho(x, y)$, with functional form given by a sum (**c**) and product (**e**) of cosines, and a wavevector magnitude $Q^* = 0.265$ r.l.u. (black bars indicate the period and direction of the spatial modulation, expressed in terms of the lattice parameter $a = 3.86$ Å). The blue rectangles denote the undistorted unit cell. **d**,**f**, Fourier transforms of **c**,**e**, respectively, with Gaussian broadening. The arrows indicate the directions of the data in **a**,**b**, which validate the scenario in **c**,**d**, and not in **e**,**f**.

$Q^* = 0.265$ (r.l.u.) are given by $\Delta\rho(x,y) = \cos(Q^*x) + \cos(Q^*y)$ (Fig. 1c) and $\Delta\rho(x,y) = \cos(Q^*x) \times \cos(Q^*y)$ (Fig. 1e). The first case corresponds to reciprocal-space features along the $(H, 0)$ and $(0, H)$ axes (Fig. 1d), whereas the second yields spatial frequencies along the (H, H) and $(H, -H)$ direction (Fig. 1f). Similar Q-space patterns would be obtained in the case of alternating stripes. As no CDW peaks are observed along (H, H), we conclude that the the second scenario can be ruled out, thus establishing that charge modulations exclusively run parallel to the Cu–O bond directions (**a** and **b** axes).

The second and main part of this study focuses on the **k**-structure of the CDW order, which controls the local arrangement of excess charges within each CuO_4 plaquette. RXS is able to probe the local charge density $\Delta\rho(\mathbf{r})$ through the spatial modulation of the core (Cu-2p) to valence (Cu-3d) transition energies $\Delta E(\mathbf{r})$ (refs 18,40). Most importantly, the local symmetry of the valence orbitals (Cu-3d and O-2p) is imprinted onto the scattering tensor, which ultimately determines the observed RXS signal (see Supplementary Information for a more detailed derivation). To evaluate the symmetry of the CDW order Δ_{CDW}, we selectively probe the different transition channels (Cu-2$p_{x,y,z} \rightarrow 3d$) by rotating the light polarization in the RXS measurements. This procedure allows one to reconstruct the scattering tensor and disentangle the contributions from the different symmetry components of $\Delta_{\mathrm{CDW}}(\mathbf{k}, \mathbf{Q}) = \langle c^{\dagger}_{\mathbf{k}+\mathbf{Q}/2} \cdot c_{\mathbf{k}-\mathbf{Q}/2} \rangle$ (refs 28,41), namely: a site-centred modulation ($\Delta_{\mathrm{CDW}} = \Delta_s$), corresponding to an extra charge residing on the Cu-3d orbital (Fig. 2a); an extended s'-wave bond order [$\Delta_{\mathrm{CDW}} = \Delta_{s'}(\cos k_x + \cos k_y)$], where the spatially modulated density is on the O-2p states, and the maxima along the x and y directions coincide (Fig. 2b); and a d-wave bond order [$\Delta_{\mathrm{CDW}} = \Delta_d(\cos k_x - \cos k_y)$], where the charge modulation changes sign between x- and y-coordinated oxygen atoms, and the maxima are shifted by a half wavelength (Fig. 2c).

In the experiments we use a special geometry, in which the sample is rotated around the ordering vector $\mathbf{Q}^*$ (Fig. 3a,b). This method allows one to look at the same wavevector while modulating (as a function of the azimuthal rotation angle α) the relative weight of the Cu $2p_{x,y,z} \rightarrow 3d$ transitions, which is controlled by the light polarization through dipole selection rules. Here the α dependence of the charge-order intensity is the new information that allows one to evaluate—through comparison with theoretical predictions from scattering theory—what is the optimal mix of the s-, s'- and

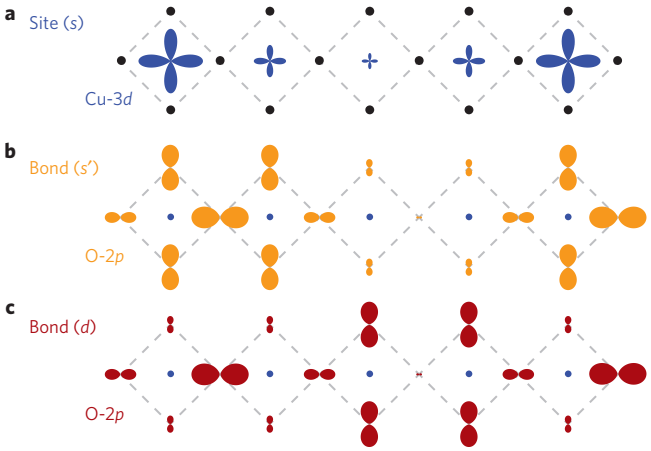

Figure 2 | Charge modulation symmetry components. a–**c**, Real-space schematics of the electronic density $\rho = \bar{\rho} + \delta\rho$ in the case of site order (charges on Cu) (**a**), or bond order (charges on O) with either extended s-wave (**b**) or d-wave (**c**) local symmetry along a single crystallographic direction.

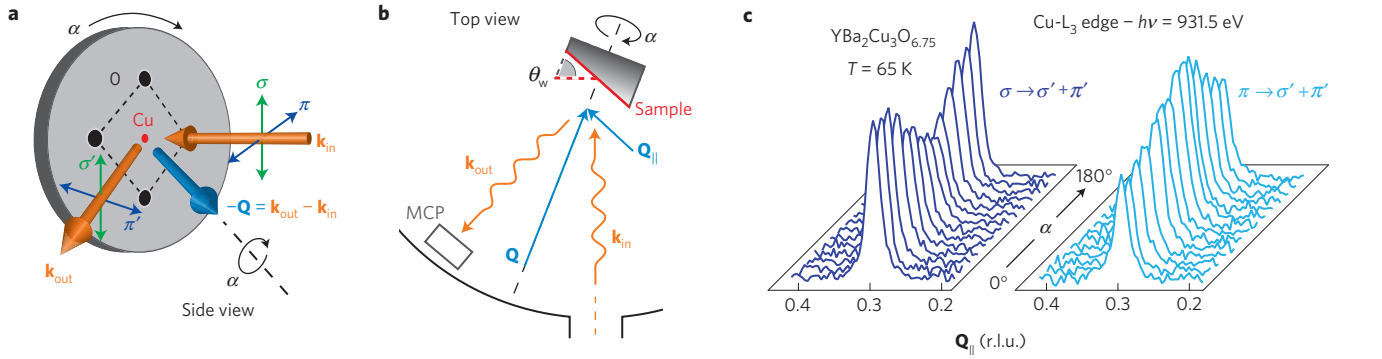

Figure 3 | Azimuthal angle-dependent RXS measurements: geometry and experimental data. a, Side view of the experimental geometry; control variables are: the incoming and outgoing photon wavevectors $\mathbf{k}_{in}$ and $\mathbf{k}_{out}$, which determine the exchanged momentum $\mathbf{Q}$; the incoming (linear) polarization $\boldsymbol{\epsilon}_{in}$ ($=\sigma$ or π); and the azimuthal angle α, whose rotation axis $\hat{\mathbf{u}}_\alpha$ coincides with the direction of $\mathbf{Q}$. The polarization of scattered X-rays (σ' or π') is not analysed. **b**, Top view, illustrating the need for a wedge-shaped sample holder to guarantee the condition $\hat{\mathbf{u}}_\alpha \| \mathbf{Q}$ for the specific $\mathbf{Q}$-vector of interest ($\theta_w = 57.5°$ and 62° for YBCO and Bi2201, respectively). The full (dashed) red line defines the geometry corresponding to $\alpha = 0°$ ($\alpha = 180°$). Scattered photons are collected using a multichannel-plate (MCP) detector. **c**, Azimuthal angle-dependent $\mathbf{Q}$-scans of the CDW peak (after subtraction of fluorescence background) at $\mathbf{Q}_{CDW} = (0, 0.31, 1.5)$ in YBCO-Ortho III, plotted versus the CuO_2-plane projection of the exchanged momentum $\mathbf{Q}_\|$.

d-wave symmetry terms that best reproduces the experimental results via their contribution within the scattering tensor. The azimuthal dependence of the RXS signal was studied in Bi2201-UD15K, at $\mathbf{Q}^* \sim (0.265, 0, 2.8)$, and in two underdoped $YBa_2Cu_3O_y$ compounds: $YBa_2Cu_3O_{6.51}$ (YBCO-Ortho II, with $p \simeq 0.10$) and $YBa_2Cu_3O_{6.75}$ (YBCO-Ortho III, with $p \simeq 0.13$), at $\mathbf{Q}^* \sim (0, 0.31, 1.5)$. A series of in-plane momentum ($\mathbf{Q}_\|$) scans of the charge-order peak in YBCO-Ortho III, acquired at $T = T_c = 75$ K with both σ- and π-polarized incoming X-rays, is presented in Fig. 3c for the range $0° < \alpha < 180°$, where $\alpha = 0$ corresponds to having the **b** axis in the scattering plane (as determined by high-energy Bragg diffraction) in the configuration of Fig. 4b (full red line).

The total scattered intensity I_{RXS} is extracted by fitting the RXS momentum scans with a Gaussian peak, and is in general proportional to the amplitude of the charge modulation. As described in equation (1) below, we can directly compare I_{RXS} to the theoretical scattering tensor F_{pq} (refs 42,43):

$$I_{\epsilon\to\epsilon'}(\mathbf{Q}^*, \alpha) \propto \left| \sum_{pq} \epsilon_p \cdot F_{pq}(\mathbf{Q}^*, \alpha) \cdot \epsilon'_q \right|^2 \quad (1)$$

where $\boldsymbol{\epsilon}$ and $\boldsymbol{\epsilon}'$ represent the polarization vectors for incoming and outgoing photons, respectively, while $\mathbf{Q}^*$ is the ordering wavevector. The α dependence is induced by simply applying a rotation (about the azimuthal axis and of magnitude equal to α) to the scattering tensor F_{pq}. Based on symmetry arguments (see Supplementary Information for additional details) the unrotated scattering tensor F_{pq} can be written in terms of a linear combination of the s-, s'- and d-wave components of the charge order, with respective magnitudes δ_s, $\delta_{s'}$ and δ_d [note that, as the scattering yield at the Cu-L_3 edge is more sensitive to charges on the Cu site (s-wave order) than on the O site (s'- and d-wave order), we have that $\delta_d/\delta_{s'} = \Delta_d/\Delta_{s'}$, whereas in general $\delta_s/\delta_d > \Delta_s/\Delta_d$ and $\delta_s/\delta_{s'} > \Delta_s/\Delta_{s'}$; see Supplementary Information for more details]. This way F_{pq} becomes:

$$F_{pq}(\pm\mathbf{Q}^*) = \begin{vmatrix} \delta_s + (\delta_{s'} + \delta_d)\cos\phi & 0 & 0 \\ 0 & \delta_s + \delta_{s'} - \delta_d & 0 \\ 0 & 0 & \gamma\delta_s \end{vmatrix} \quad (2)$$

where the phase $\phi = Q^* \cdot a/2$ accounts for the mismatch between the ordering period and the lattice parameter, while γ is the ratio between the out-of-plane and the in-plane transition matrix elements, which has been estimated from X-ray absorption data on Bi2201 (a similar analysis in YBCO is hampered by the proximity between the chain and plane transitions in the absorption spectrum). Note that a similar version of equation (2), developed here for the Cu-L edge, has been recently used in ref. 39 for RXS at the O-K edge.

The total calculated scattering intensity, before self-absorption correction, is then given by: $I_{calc}(\alpha) = I_{\epsilon\to\sigma'}(\alpha) + I_{\epsilon\to\pi'}(\alpha)$, where $\epsilon = \sigma$ or π. We subsequently include self-absorption corrections on the calculated profiles (see Supplementary Information). Figure 4 presents the experimental data for the two YBCO samples and for Bi2201 in the form of the RXS intensity ratio between vertical and horizontal polarization configurations $I^\sigma_{RXS}/I^\pi_{RXS}$ (grey markers) to factor out possible extrinsic effects due to the sample shape and orientation with respect to the scattering geometry. Also shown are model calculations (I_{calc}, continuous lines) for all possible combinations of two CDW symmetry components—that is, $s+d$, $s'+d$ and $s+s'$—together with the pure d-wave model for comparison (for a complete analysis of all possible combinations of one- and two-symmetry terms see Supplementary Methods). In particular, the peculiarity of those combinations including a d-wave term is that the minimum in the calculated profile $I^\sigma_{calc}/I^\pi_{calc}$ is displaced from $\alpha = 90°$, a consequence of the more strongly asymmetric pattern of charges within each CuO_4 plaquette (see Fig. 2). In contrast, a combination of s and s' components alone remains symmetric with respect to $\alpha = 90°$, and so do the pure-symmetry profiles. As the experimental data are characterized by a slight asymmetry ($\alpha_{min} \simeq 100°$), the two-component combinations involving a locally asymmetric (d-wave) term fit the YBCO data more closely. For such combinations, the presence of a symmetric term is also found to be necessary, as a pure d-wave fit clearly overestimates the total amplitude of the experimental azimuthal modulation (see dotted grey line in Fig. 4).

On the other hand, the lack of a clear asymmetry in Bi2201 prevents our analysis from providing a conclusive answer on the symmetry of charge order in this material. However, such an asymmetry might be overshadowed by the larger scatter in the data due to weaker CDW features in RXS data on Bi-cuprates than in YBCO. Indeed, we note that this has been assessed—for (bilayer) Bi-based cuprates—using alternative approaches[38].

The qualitative argument based on the data asymmetry is supported by a more quantitative assessment of the likelihood of each model, which was estimated by evaluating the reduced chi-square (χ^2_{red}) for all the experimental points and theoretical configurations shown in Fig. 4 (see Supplementary Information for

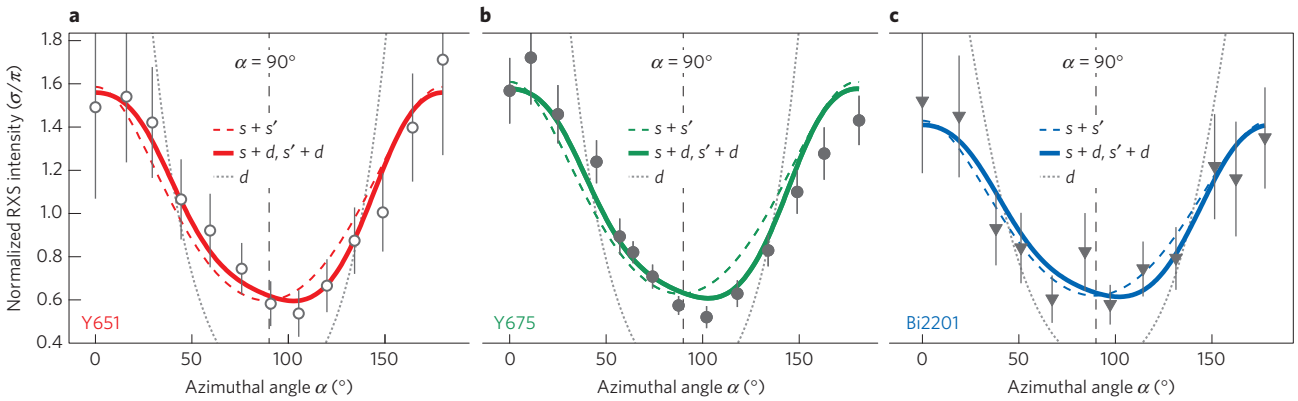

Figure 4 | Experimental and calculated CDW peak intensity versus azimuthal angle. a–c, Normalized RXS intensity ratio $I^{\sigma}_{RXS}/I^{\pi}_{RXS}$ for Y651 (**a**), Y675 (**b**) and Bi2201 (**c**). The vertical error bars are obtained by propagation of the uncertainties for the σ and π RXS intensities as obtained from a nonlinear least-squares regression analysis of the raw experimental data. Theoretical profiles for three possible two-component combinations are obtained from a least-squares fitting method and overlaid to the data: $s+d$ and $s'+d$ (full, a single trace is used as the resulting profiles are nearly overlapping), and $s+s'$ (dashed). Best-fit, pure d-wave azimuthal profiles are also shown as dotted grey curves. For all data points the uncertainty on the azimuthal angle is given as $\sigma_{\alpha} \sim 3°$. The vertical dashed lines mark the azimuthal position $\alpha = 90°$.

a formal definition of χ^2_{red}). The values of χ^2_{red} are subsequently used within the chi-squared cumulative distribution function to extract the probability P for the different models considered here, where P denotes the probability that the model under consideration yields a better agreement than a data set randomly generated from a normal distribution (with mean-square deviations equal to the experimental uncertainties). These probability levels (Table 1) indicate that a symmetry decomposition including a dominant d-wave bond-order component is more likely to describe the experimental data from YBCO than a combination of symmetric s- and s'-wave components. Although the relative magnitude of the d- versus s- or s'-wave character here is not strongly constrained, we note the presence of a symmetric component of about 20% of the total charge order (see Table 1 and Supplementary Methods for a more detailed discussion on the analysis); this closely follows theoretical predictions for Δ_{CDW} in the context of the t–J model[28,41,44], as well as recent STM results[38]. Finally, we also note the close proximity between a mixed solution with prevailing d-wave character and those with prevailing s- or s'-wave character; this is illustrated in Supplementary Fig. 6, which however indicates that even in the latter case the d-wave component would still be as large as 20–30%.

Altogether, in YBCO we reveal the charge-ordered electronic ground state to be best described by a bond order with the modulating charge mainly located on O-2p orbitals and characterized by a prominent d-wave character, whereas in Bi2201 the absence of charge-order features along the diagonal axes in momentum space demonstrates that charge modulations propagate exclusively along the **a** and **b** axes. Therefore, our study reaffirms the pivotal role played by the O-2p ligand states in hole-doped cuprates[45,46]. In light of STM works pointing to bond order in $Ca_{1.88}Na_{0.12}CuO_2Cl_2$ and $Bi_2Sr_2CaCu_2O_{8+\delta}$ (refs 47,48), and more recently revealing a dominant d-wave symmetry[38], we propose that in the Bi-, Y- and Cl-based cuprates, which all exhibit a very similar charge-order phenomenology, the microscopic defining symmetry contains a prominent d-wave bond-order component. In the La-based cuprates, which already exhibit a doping dependence for the charge-ordering vectors opposite to that of Bi2201 and YBCO (ref. 19), a recent detailed study has revealed a predominant s'-wave bond-order[39], suggesting a different manifestation of the charge-order symmetry in these systems. In such a context, we anticipate that future work will be needed to provide further experimental constraints to the ratio of different symmetry terms, to understand the sensitivity of different probes to the symmetry of the charge order, and possibly also how the latter is modulated by the out-of-plane component of the wavevector.

The commonality between the symmetry of the superconducting (SC) and CDW orders might suggest that the same attractive interaction responsible for particle–particle (Cooper) pairing might also be active in the particle–hole channel. This aspect—which has been recently proposed at the theoretical level and was suggested to originate from the exchange part (J) of the interaction Hamiltonian[28,29,41,44]—is here corroborated by our experiments. This has deep implications in the context of the competing instabilities of the electronic system and for an ultimate understanding of the pairing mechanism.

Table 1 | Statistical comparison of CDW models.

Sample	Order Ratio	$s+s'$ s'/s	$s+d$ s/d	$s'+d$ s'/d
Y651		0.01	0.21	0.27
Y675		−0.01	0.22	0.27
Probability level P		5.6	83.8	85.5

Best-fit component ratios s'/s, s/d and s'/d for binary combinations of the fundamental CDW symmetry terms $s+s'$, $s+d$ and $s'+d$, respectively. Probability levels P for the hypothesis that each specific CDW model fits the experimental data better than a random sample. The values suggest that those combinations featuring a prominent d-wave bond-order component manifest a great likelihood ($P > 90\%$) of reproducing the experimental data.

Methods

Methods and any associated references are available in the online version of the paper.

Received 5 February 2014; accepted 16 April 2015; published online 25 May 2015

References

1. Yoshizawa, H., Kawano, H., Tomioka, Y. & Tokura, Y. Neutron-diffraction study of the magnetic-field-induced metal–insulator transition in $Pr_{0.7}Ca_{0.3}MnO_3$. *Phys. Rev. B* **52,** R13145–R13148 (1995).
2. Tranquada, J. M., Buttrey, D. J. & Sachan, V. Incommensurate stripe order in $La_{2-x}Sr_xNiO_4$ with $x = 0.225$. *Phys. Rev. B* **54,** 12318–12323 (1996).
3. Cwik, M. *et al.* Magnetic correlations in $La_{2-x}Sr_xCoO_4$ studied by neutron scattering: Possible evidence for stripe phases. *Phys. Rev. Lett.* **102,** 057201 (2009).

4. Tranquada, J. M., Sternlieb, B. J., Axe, J. D., Nakamura, Y. & Uchida, S. Evidence for stripe correlations of spins and holes in copper oxide superconductors. *Nature* **375,** 561–563 (1995).
5. v. Zimmermann, M. *et al.* Hard X-ray diffraction study of charge stripe order in $La_{1.48}Nd_{0.4}Sr_{0.12}CuO_4$. *Europhys. Lett.* **41,** 629–634 (1998).
6. Abbamonte, P. *et al.* Spatially modulated 'Mottness' in $La_{2-x}Ba_xCuO_4$. *Nature Phys.* **1,** 155–158 (2005).
7. Fink, J. *et al.* Charge ordering in $La_{1.8-x}Eu_{0.2}Sr_xCuO_4$ studied by resonant soft x-ray diffraction. *Phys. Rev. B* **79,** 100502 (2009).
8. Poilblanc, D. & Rice, T. M. Charged solitons in the Hartree–Fock approximation to the large-U Hubbard model. *Phys. Rev. B* **39,** 9749–9752 (1989).
9. Zaanen, J. & Gunnarsson, O. Charged magnetic domain lines and the magnetism of high-T_c oxides. *Phys. Rev. B* **40,** 7391–7394 (1989).
10. Machida, K. Magnetism in La_2CuO_4 based compounds. *Physica C* **158,** 192–196 (1989).
11. Emery, V. J., Kivelson, S. A. & Lin, H. Q. Phase separation in the t–J model. *Phys. Rev. Lett.* **64,** 475–478 (1990).
12. Castellani, C., Di Castro, C. & Grilli, M. Singular quasiparticle scattering in the proximity of charge instabilities. *Phys. Rev. Lett.* **75,** 4650–4653 (1995).
13. Hoffman, J. E. *et al.* A four unit cell periodic pattern of quasi-particle states surrounding vortex cores in $Bi_2Sr_2CaCu_2O_{8+\delta}$. *Science* **295,** 466–469 (2002).
14. Howald, C., Eisaki, H., Kaneko, N. & Kapitulnik, A. Coexistence of periodic modulation of quasiparticle states and superconductivity in $Bi_2Sr_2CaCu_2O_{8+\delta}$. *Proc. Natl Acad. Sci. USA* **100,** 9705–9709 (2003).
15. Wu, T. *et al.* Magnetic-field-induced charge-stripe order in the high-temperature superconductor $YBa_2Cu_3O_y$. *Nature* **477,** 191–194 (2011).
16. Ghiringhelli, G. *et al.* Long-range incommensurate charge fluctuations in $(Y,Nd)Ba_2Cu_3O_{6+x}$. *Science* **337,** 821–825 (2012).
17. Chang, J. *et al.* Direct observation of competition between superconductivity and charge density wave order in $YBa_2Cu_3O_y$. *Nature Phys.* **8,** 871–876 (2012).
18. Achkar, A. J. *et al.* Distinct charge orders in the planes and chains of ortho-III ordered $YBa_2Cu_3O_{6+\delta}$ superconductors identified by resonant elastic X-ray scattering. *Phys. Rev. Lett.* **109,** 167001 (2012).
19. Blackburn, E. *et al.* X-ray diffraction observations of a charge-density-wave order in superconducting ortho-II $YBa_2Cu_3O_{6.54}$ single crystals in zero magnetic field. *Phys. Rev. Lett.* **110,** 137004 (2013).
20. Blanco-Canosa, S. *et al.* Momentum-dependent charge correlations in $YBa_2Cu_3O_{6+\delta}$ superconductors probed by resonant X-ray scattering: Evidence for three competing phases. *Phys. Rev. Lett.* **110,** 187001 (2013).
21. Le Tacon, M. *et al.* Giant phonon anomalies and central peak due to charge density wave formation in $YBa_2Cu_2O_{6.6}$. *Nature Phys.* **10,** 52–58 (2014).
22. Comin, R. *et al.* Charge order driven by Fermi-arc instability in $Bi_2Sr_{2-x}La_xCuO_{6+\delta}$. *Science* **343,** 390–392 (2014).
23. da Silva Neto, E. *et al.* Ubiquitous interplay between charge ordering and high-temperature superconductivity in cuprates. *Science* **343,** 393–396 (2014).
24. da Silva Neto, E. H. *et al.* Charge ordering in the electron-doped superconductor $Nd_{2-x}Ce_xCuO_4$. *Science* **347,** 282–285 (2015).
25. Kivelson, S. A. *et al.* How to detect fluctuating stripes in the high-temperature superconductors. *Rev. Mod. Phys.* **75,** 1201–1241 (2003).
26. Seibold, G., Grilli, M. & Lorenzana, J. Stripes in cuprate superconductors: Excitations and dynamic dichotomy. *Physica C* **481,** 132–145 (2012).
27. Efetov, K. B., Meier, H. & Pépin, C. Pseudogap state near a quantum critical point. *Nature Phys.* **9,** 442–446 (2013).
28. Sachdev, S. & La Placa, R. Bond order in two-dimensional metals with antiferromagnetic exchange interactions. *Phys. Rev. Lett.* **111,** 027202 (2013).
29. Davis, J. C. S. & Lee, D-H. Concepts relating magnetic interactions, intertwined electronic orders, and strongly correlated superconductivity. *Proc. Natl Acad. Sci. USA* **110,** 17623–17630 (2013).
30. Meier, H., Einenkel, M., Pépin, C. & Efetov, K. B. Effect of magnetic field on the competition between superconductivity and charge order below the pseudogap state. *Phys. Rev. B* **88,** 020506 (2013).
31. He, Y., Scherpelz, P. & Levin, K. Theory of fluctuating charge ordering in the pseudogap phase of cuprates via a preformed pair approach. *Phys. Rev. B* **88,** 064516 (2013).
32. Bulut, S., Atkinson, W. A. & Kampf, A. P. Spatially modulated electronic nematicity in the three-band model of cuprate superconductors. *Phys. Rev. B* **88,** 155132 (2013).
33. Nie, L., Tarjus, G. & Kivelson, S. A. Quenched disorder and vestigial nematicity in the pseudogap regime of the cuprates. *Proc. Natl Acad. Sci. USA* **111,** 7980–7985 (2014).
34. Dalla Torre, E. G., He, Y., Benjamin, D. & Demler, E. Exploring quasiparticles in high-T_c cuprates through photoemission, tunneling, and X-ray scattering experiments. *New J. Phys.* **111,** 022001 (2015).
35. Lee, P. A. Amperean pairing and the pseudogap phase of cuprate superconductors. *Phys. Rev. X* **4,** 031017 (2014).
36. Wang, Y. & Chubukov, A. Charge-density-wave order with momentum $(2q,0)$ and $(0,2q)$ within the spin-fermion model: Continuous and discrete symmetry breaking, preemptive composite order, and relation to pseudogap in hole-doped cuprates. *Phys. Rev. B* **90,** 035149 (2014).
37. Melikyan, A. & Norman, M. R. Symmetry of the charge density wave in cuprates. *Phys. Rev. B* **89,** 024507 (2014).
38. Fujita, K. *et al.* Direct phase-sensitive identification of a d-form factor density wave in underdoped cuprates. *Proc. Natl Acad. Sci. USA* **111,** E3026–E3032 (2014).
39. Achkar, A. J. *et al.* Orbital symmetry of charge density wave order in $La_{1.875}Ba_{0.125}CuO_4$ and $YBa_2Cu_3O_{6.67}$. Preprint at http://arXiv:1409.6787 (2014).
40. Achkar, A. J. *et al.* Resonant X-ray scattering measurements of a spatial modulation of the Cu 3d and O 2p energies in stripe-ordered cuprate superconductors. *Phys. Rev. Lett.* **110,** 017001 (2013).
41. Metlitski, M. A. & Sachdev, S. Quantum phase transitions of metals in two spatial dimensions. II. Spin density wave order. *Phys. Rev. B* **82,** 075128 (2010).
42. Schüßler-Langeheine, C. *et al.* Spectroscopy of stripe order in $La_{1.8}Sr_{0.2}NiO_4$ using resonant soft X-ray diffraction. *Phys. Rev. Lett.* **95,** 156402 (2005).
43. Matteo, S. D. Resonant x-ray diffraction: Multipole interpretation. *J. Phys. D: Appl. Phys.* **45,** 163001 (2012).
44. Vojta, M. & Rösch, O. Superconducting d-wave stripes in cuprates: Valence bond order coexisting with nodal quasiparticles. *Phys. Rev. B* **77,** 094504 (2008).
45. Zaanen, J., Sawatzky, G. A. & Allen, J. W. Band gaps and electronic structure of transition-metal compounds. *Phys. Rev. Lett.* **55,** 418–421 (1985).
46. Emery, V. J. & Reiter, G. Reply to "Validity of the t–J model". *Phys. Rev. B* **41,** 7247–7249 (1990).
47. Kohsaka, Y. *et al.* An intrinsic bond-centered electronic glass with unidirectional domains in underdoped cuprates. *Science* **315,** 1380–1385 (2007).
48. Lawler, M. J. *et al.* Intra-unit-cell electronic nematicity of the high-T_C copper-oxide pseudogap states. *Nature* **466,** 347–351 (2010).

Acknowledgements

We are grateful to J. E. Hoffman, Y. He and M. Yee for sharing their STM data and for fruitful discussions. We also acknowledge M. Le Tacon, S. Sachdev, M. Norman, S. Kivelson, C. Pepin, E. D. Torre and E. Demler for insightful discussions. This work was supported by the Max Planck—UBC Centre for Quantum Materials, the Killam, A. P. Sloan, A. von Humboldt, and NSERC's Steacie Memorial Fellowships (A.D.), the Canada Research Chairs Program (A.D., G.A.S.), NSERC, CFI and CIFAR Quantum Materials. Part of the research described in this paper was performed at the Canadian Light Source, which is funded by the CFI, NSERC, NRC, CIHR, the Government of Saskatchewan, WD Canada and the University of Saskatchewan. R.C. acknowledges the receipt of support from the CLS Graduate Student Travel Support Program. E.H.d.S.N. acknowledges support from the CIFAR Global Academy.

Author contributions

R.C., B.K., G.A.S. and A.D. conceived this investigation. R.C. performed RXS measurements at the Canadian Light Source with the assistance of R.S., F.H., E.H.d.S.N. and L.C. R.C. developed the theoretical model and performed related calculations. R.C., A.F., A.J.A., D.G.H., B.K., G.A.S. and A.D. are responsible for data analysis and interpretation. R.L., W.N.H. and D.A.B. provided the YBCO samples. Y.Y. and H.E. provided the Bi2201 samples. All of the authors discussed the underlying physics and contributed to the manuscript. R.C. and A.D. wrote the manuscript. A.D. is responsible for overall project direction, planning and management.

Additional information

Supplementary information is available in the online version of the paper. Reprints and permissions information is available online at www.nature.com/reprints. Correspondence and requests for materials should be addressed to R.C. or A.D.

Competing financial interests

The authors declare no competing financial interests.

Methods

Sample characterization. This study focuses on two underdoped $YBa_2Cu_3O_{6+y}$ single crystals ($y=0.51$, $p\simeq 0.10$, $T_c=57$ K, YBCO-Ortho II; $y=0.75$, $p\simeq 0.13$, $T_c=75$ K, YBCO-Ortho III) and one underdoped crystal of $Bi_2Sr_{1.2}La_{0.8}CuO_{6+\delta}$ ($p\sim 0.11$, $T_c=15$ K, Bi2201-UD15K). The superconducting critical temperature T_c was determined from magnetic susceptibility measurements. The T_c-to-doping correspondence is taken from ref. 49 (YBCO) and ref. 50 (Bi2201).

Soft X-ray scattering. The scattering measurements were performed at beamline REIXS of the Canadian Light Source, on a 4-circle diffractometer in a 10^{-10} mbar ultrahigh-vacuum chamber, with a photon flux around 5×10^{12} photons s^{-1} and $\Delta E/E\sim 2\times 10^{-4}$ energy resolution. In addition, fully polarized incoming light is used, with two available configurations: σ (polarization vector perpendicular to the scattering plane) or π (polarization vector in the scattering plane). Owing to poor performance of polarization analysers in the soft X-ray regime, the polarization of the scattered light was not resolved in any of the measurements. To maximize the charge order signal, all measurements were taken at the peak energy of the Cu-L_3 edge ($h\nu=931.5$ eV) and at the superconducting transition temperature T_c. The azimuthal angle α is defined as the angle between the RXS scan direction in the (Q_x, Q_y) plane of momentum space and the crystallographic **b** axis (for more details on the azimuthal sample geometry see Supplementary Fig. 1 and the corresponding discussion in the Supplementary Information). Note that, at all azimuthal angles, the sample tilt angle has been slightly readjusted to ensure that the RXS scans slice across the maximum of the CDW peak.

References

49. Liang, R., Bonn, D. A. & Hardy, W. N. Evaluation of CuO_2 plane hole doping in $YBa_2Cu_3O_{6+x}$ single crystals. *Phys. Rev. B* **73,** 180505 (2006).
50. Ando, Y. *et al.* Carrier concentrations in $Bi_2Sr_{2-z}La_zCuO_{6+\delta}$ single crystals and their relation to the Hall coefficient and thermopower. *Phys. Rev. B* **61,** R14956–R14959 (2000).